tive repression via recruitment of specific HDACs and gene silencing by recruitment of CoREST complexes (*10–12*) to specific promoters in a cell type– and promoter-specific DNA methylation manner.

Similar events occur in vivo, with CoREST, MeCP2, and $K^{m}9H3$ markers of silencing proving to be present on the *NaCh II* promoter in adult murine liver and heart (Fig. 5A). With the use of MEME and SP-STAR motif–finding algorithms (*38*), we located two motifs that are present preferentially within 250 bp of an experimentally confirmed RE1/NRSE consensus site that may be related to the known RE1/NRSE consensus site (fig. S7). The full importance of these motifs will need to be genetically studied, but one (RE2) is capable of both transcriptional repression and REST/NRSF binding (*14*). Thus, analogous to nucleation of gene silencing at specific sequences [polycomb group response elements (PREs)] (2), we suggest that the RE1/NRSE element, perhaps in concert with related sites, might nucleate silencing of specific chromosomal regions.

Recruitment of the corepressor CoREST to REST/NRSE gene targets appears to act as a molecular beacon for the silencing machinery, including MeCP2, SUV39H1, and HP1, to propagate and maintain a methyl CpG-dependent silent state across specific chromosomal intervals, including genes that do not contain REST/NRSF-binding sites (Fig. 5B). This model is consistent with observations that DNA methylation by itself is not sufficient for silencing (*41*). MeCP2 appears to be a critical component of these events in Rat-1 cells, but other factors may operate in cell types where MeCP2 is not expressed. The recruitment of SUV39H1, in part via interactions with MeCP2 complexes, apparently leads to HP1 recruitment and chromatin condensation in cultured cells and in vivo (Fig. 5B). The presence of $K^{m}9$ but not $K^{m}4$ histone H3 across the rCh3 q22-34 region is consistent with CoREST-mediated recruitment of silencing machinery and the proposed epigenetic program (*27*, *28*, *31*, *35*, *39*).

These observations further suggest that other factors analogous to REST are likely to mediate the silencing of distinct chromosomal regions that regulate other biological programs, some via recruitment of CoREST complexes. Conversely, the expression of REST/NRSF early in brain development and the potential silencing of genes such as $SMARC_E$ suggest that REST/NRSF may also control important roles in early embryonic gene silencing.

References and Notes

1. E. J. Richards, S. C. Elgin, *Cell* **108**, 489 (2002).
2. C. J. Schoenherr, D. Anderson, *Science* **267**, 1360 (1995).
3. J. A. Chong *et al.*, *Cell* **80**, 949 (1995).
4. C. J. Schoenherr, A. J. Paquette, D. J. Anderson, *Proc. Natl. Acad. Sci. U.S.A.* **93**, 988 (1996).
5. N. Mori, R. Stein, D. Sigmund, D. J. Anderson, *Neuron* **4**, 583 (1990).
6. N. Ballas *et al.*, *Neuron* **31**, 353 (2001).
7. Y. Naruse, T. Aoki, T. Kojima, N. Mori, *Proc. Natl. Acad. Sci. U.S.A.* **96**, 13691 (1999).
8. K. Jepsen *et al.*, *Cell* **102**, 753 (2000).
9. M. E. Andres *et al.*, *Neuron* **96**, 9873 (1999).
10. A. You, J. K. Tong, C. M. Grozinger, S. L. Schreiber, *Proc. Natl. Acad. Sci. U.S.A.* **98**, 1454 (2001).
11. G. W. Humphrey *et al.*, *J. Biol. Chem.* **276**, 6817 (2001).
12. M. A. Hakimi *et al.*, *Proc. Natl. Acad. Sci. U.S.A.* **99**, 7420 (2002).
13. Materials and methods are available as supporting material at *Science* Online.
14. V. V. Lunyak *et al.*, unpublished data.
15. A. Razin, M. Szyf, *Biochim. Biophys. Acta* **782**, 331 (1989).
16. S. Tweedie, S. Charlton, V. Clark, A. Bird, *Mol. Cell. Biol.* **17**, 1469 (1997).
17. M. Brandies, M. Ariel, H. Cedar, *Bioassays* **15**, 709 (1993).
18. P. H. Tate, A. Bird., *Curr. Opin. Genet. Dev.* **3**, 226 (1993).
19. Z. Siegfried, S. Eden, M. Mendelsohn, X. Feng, B. Z. Tsuberi, H. Cedar, *Nature Genet.* **22**, 203 (1999).
20. J. D. Lewis *et al.*, *Cell* **69**, 905 (1992).
21. M. C. Lorincz, D. Schubeler, M. Groudine, *Mol. Cell. Biol.* **21**, 7913 (2001).
22. R. E. Amir *et al.*, *Nature Genet.* **23**, 185 (1999).
23. R. X. Chen, S. Akbarian, M. Tudor, R. Jaenisch, *Nature Genet.* **27**, 327 (2001).
24. A. C. Bell, G. Felsenfeld, *Nature* **405**, 482 (2000).
25. K. Kokura *et al.*, *J. Biol. Chem.* **276**, 34115 (2001).
26. R. I. Gregory *et al.*, *Mol. Cell. Biol.* **21**, 5426 (2001).
27. E. Heard *et al.*, *Cell* **107**, 727 (2001).
28. S. Rea *et al.*, *Nature* **406**, 593 (2000).
29. K. Mechtler, C. P. Ponting, C. D. Allis, T. Jenuwein, *Nature* **406**, 593 (2000).
30. J. C. Rice, C. D. Allis, *Curr. Opin. Cell Biol.* **13**, 263 (2001).
31. K. Noma, C. D. Allis, S. I. Grewal, *Science* **293**, 1150 (2001).
32. A. J. Bannister *et al.*, *Nature* **410**, 120 (2001).
33. M. D. Litt, M. Simpson, M. Gaszner, C. D. Allis, G. Felsenfeld, *Science* **293**, 2453 (2001).
34. M. Lachner, D. O'Carroll, S. Rea, K. Mechtler, T. Jenuwein, *Nature* **410**,116 (2001).
35. J. Nakayama, A. J. Klar, S. I. Grewal, *Cell* **101**, 307 (2000).
36. J. Nakayama, J. C. Rice, B. D. Strahl, C. D. Allis, S. I. Grewal, *Science* **292**, 10 (2001).
37. P. A. Pevzner, S. H. Sze, *Intelligent Systems in Molecular Biology* (AAAI Press, La Jolla, CA, 2000), pp. 269–278.
38. M. Mieda, T. Haga, D. W. Saffeen, *J. Biol. Chem.* **272**, 5854 (1997).
39. I. C. Wood, A. Roopra, N. J. Buckley, *J. Biol. Chem.* **271**, 14221 (1996).
40. T. Jenuwein, C. D. Allis, *Science* **293**, 1074 (2001).
41. P. Jones, *Nature Rev. Genet.* **3**, 415 (2002).

42. We particularly thank A. Gonzalez (Santa Cruz Biotech Inc.) for helpful advice, K. Ohgi for technical assistance, and P. Myer and M. Fisher for figure and manuscript preparation. M.G.R. is an Investigator and V.L. is an Associate with HHMI. G.P. is supported by the Canadian Institute of Health Research. Supported by grants from NIH to G.M. and M.G.R. and a grant from CapCURE to M.G.R.

Supporting Online Material

www.sciencemag.org/cgi/content/full/1076469/DC1
Materials and Methods
Figs. S1 to S7

23 July 2002; accepted 23 September 2002
Published online 24 October 2002;
10.1126/science.1076469
Include this information when citing this paper.

Martian Meteorite Launch: High-Speed Ejecta from Small Craters

James N. Head,[1,2] H. Jay Melosh,[1] Boris A. Ivanov[3]

We performed high-resolution computer simulations of impacts into homogeneous and layered martian terrain analogs to try to account for the ages and characteristics of the martian meteorite collection found on Earth. We found that craters as small as ~3 kilometers can eject $\sim 10^7$ decimeter-sized fragments from Mars, which is enough to expect those fragments to appear in the terrestrial collection. This minimum crater diameter is at least four times smaller than previous estimates and depends on the physical composition of the target material. Terrain covered by a weak layer such as an impact-generated regolith requires larger, therefore rarer, impacts to eject meteorites. Because older terrain is more likely to be mantled with such material, we estimate that the martian meteorites will be biased toward younger ages, which is consistent with the meteorite collection.

Past models of the origin of the martian meteorite suite (*1–3*), which supposed that the meteorites were launched from relatively large craters, are unable to account for the presently known distribution of cosmic ray exposure (CRE) ages (*4*). Using the known present-day lunar flux of impactors, extrapolated to Mars (*5*, *6*), the probability of even one 12-km-diameter crater forming on Shergottite-age terrain is ~0.04. In contrast, CRE ages (Table 1) and petrology (*7*, *8*) indicate that the known martian meteorites were launched in six or seven events. Thus, the observed launch frequency disagrees by two orders of magnitude with the estimated cratering rate. Appeals to statistics of small numbers are unsatisfactory, given the large number of launch events now recognized.

[1]Department of Planetary Sciences, University of Arizona, 1629 East University Boulevard, Tucson, AZ 85721, USA. [2]Raytheon Missile Systems, Post Office Box 11337, Building 805, M/S L5, Tucson, AZ 85734–1337, USA. [3]Institute for the Dynamics of Geospheres, Russian Academy of Sciences, Moscow, Russia 117939.

In addition, most martian meteorites have likely crystallization ages of a few hundred million years ago (Ma), whereas about half of the martian surface is thought to date to about 3900 Ma (*8*, *9*).

Constraints from geochemistry, dynamics, and physics. The relatively young (~200 Ma) Shergottites are basaltic in composition. Estimates of the crater diameter at which the surface is saturated (*5*, *10*) indicate that the regolith thickness on this young terrain is on the order of 1 m. Older meteorites come from terrain that has had more time to accumulate a regolith. We estimate that for Nakhlite-age material, the regolith is on the order of tens of meters thick (*5*). The ancient stone ALHA84001 presumably comes from the heavily cratered ancient terrain, where the regolith thickness may be on the order of hundreds of meters (*5*). These geologic considerations determined the target model used in our calculations. The physical size of the martian meteorites as well as ablation studies determined the size of the meteorites to be less than a few decimeters before they entered Earth's atmosphere (*9*) (Table 1). Most Shergottites are shocked to pressures in the 30- to 45-GPa range. Such shock estimates are somewhat uncertain, so we presume that the stones are not shocked to melting; that is, they are shocked to less than 60 GPa.

The complete lack of evidence for 2-π cosmic ray exposure (cosmic rays that arrive from only one hemisphere) argues that the martian meteorites came from some depth in the crust, at least 1 m (*9*). To be conservative, we excluded all material within 2 m of the surface. The frequent dust storms on Mars may well cover the entire planet with a blanket of dust of a thickness of 2 m (*5*). Hence, all martian bedrock might be shielded from 2-π cosmic ray exposure. Celestial mechanics plays a significant role in this analysis. The fraction of martian ejecta that travels to Earth on a 10-million-year time scale is 5% (*11*, *12*). This material resides on Earth's surface for a finite time, typically on the order of 10^4 years (*13*). The amount of Earth's surface that is efficiently searched for meteorites is less than 0.1%. Combining these factors, we estimate that the probability of finding on Earth a fragment ejected from Mars is about 10^{-6} to 10^{-7}. Finally, to escape from Mars's gravitational field, the ejected material must have a speed greater than the escape velocity of 5 km/s.

Hence, the results of our simulations are analyzed to meet the following criteria: ejection velocity of greater than 5 km/s, material from deeper than 2 m, shock states less than 60 GPa, and fragments larger than 3 cm in diameter and in quantities of 10^6 or more. It is assumed that the martian atmosphere is a negligible barrier to meteorite launch (*14*). If any of these criteria are not met by the impact simulation, we do not consider the crater to be a candidate source for the martian meteorites in our collections.

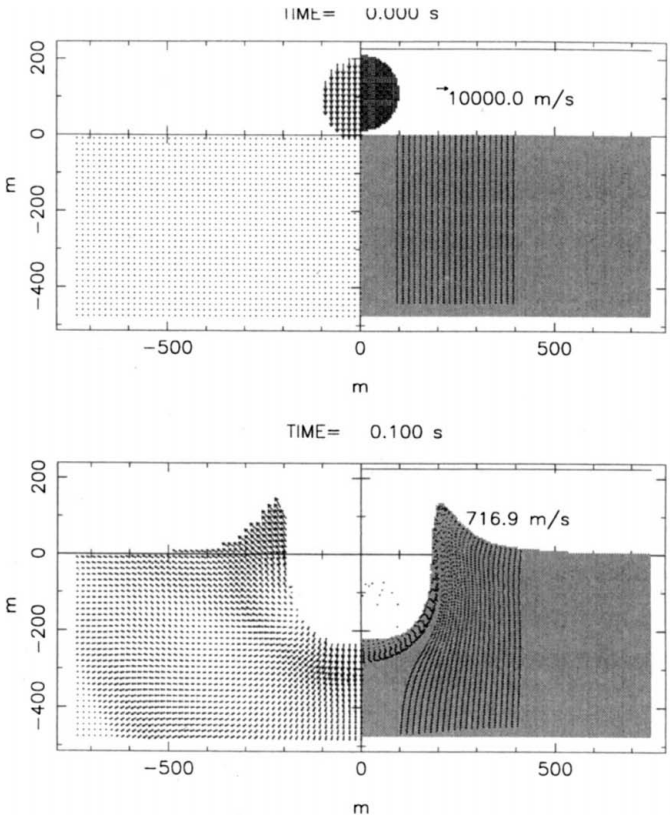

Fig. 1. The simulation begins with an Eulerian calculation shown here. A 200-m-diameter projectile strikes a surface vertically at 10 km/s. Tracer particles are imbedded in the target material and are indicated by the vertical lines. The velocity histories of the tracer particles are then used as a boundary condition for a Lagrangian simulation, wherein the fragmentation model is used to predict fragment sizes. In the Lagrangian calculation, the boundaries between different materials are well defined at all times. This is required in order to study the interference between the shock wave and the free surface.

Table 1. Selected physical and chemical data for the martian meteorites. The diameter of the implied meteoroid is calculated assuming 50% ablation and a density of 3000 kg/m^3. These are arranged in reverse order of the inferred ejection age. The ejection age is computed by combining the CRE age and the terrestrial residence age. The basaltic Shergottites and the lherzolites form distinct groups in ejection age, consistent with their differing petrology. Chassigny, though different petrologically from the Nakhlites, cannot be distinguished from them on the basis of CRE data. Sample EETA79001, the Dar al Gani stones, and sample ALH84001 are distinct from each other and the rest on the basis of ejection age. Data were compiled from (*4*, *9*, *13*, *30*–*40*). Max. P_{Sh}, shock pressure; T_{ej}, ejection age; Cpx, clinopyroxene; Opx, orthopyroxene; Ol, olivine.

Sample	Mass (kg)	Size (m)	Type	Max. P_{Sh} (GPa)	Crystallization age (Ma)	T_{ej} (Ma)
Source crater 1						
EET79001	7.94	0.22	Basalt	30–43	?	0.82 ± 0.2
Source crater 2						
DAG 476	2.015	0.14	Basalt	40–50	<400	1.2 ± 0.2
DAG 489	2.146	0.14				
(paired)	4.161	0.17				
Source crater 3						
Shergotty	4	0.17	Basalt	30–43	180	2.75 ± 0.17
Zagami	18	0.28			180	2.71 ± 0.45
QUE94201	0.012	0.03			330	2.81 ± 0.18 (2.76 ± 0.06)
Source crater 4						
ALH77005	0.483	0.08	Lherzolite	30–43	187 ± 12	3.52 ± 0.55
LEW88516	0.013	0.03		30–43	?	4.15 ± 0.62
Y793605	0.016	0.03		30–50	210 ± 62	4.4 ± 1 (3.84 ± 0.64)
Source crater 5 (and 6?)						
Nakhla	40	0.37	Cpx	–	1300	11.6 ± 1.8
Lafayette	0.8	0.10	Ol-cpx			10.1 ± 2.2
Governador Valadares	0.16	0.06	Cpx			11.4 ± 2.1 (11.0 ± 0.9)
Chassigny	4	0.17	Dunite	~35	1300	11.6 ± 1.5
Source crater 6 (7?)						
ALH84001	1.931	0.14	Opx	Complex	4500	14.4 ± 0.7

Method. We modified the SALE two-dimensional (2D) hydrocode (*15*) to incorporate fracture (*16*) and multiple materials (*17*) to model the process of mechanical spallation (*18*). We studied vertical impacts [limited by the 2D capability of the hydrocode (*19*)] at velocities ranging from 7.7 to 10 km/s (*20*), which are appropriate for asteroidal impacts on the martian surface (Fig. 1). We varied the impactor diameter from 100 to 400 m. The impactor was composed of basalt, whereas the target was either homogeneous basalt or alluvium, or a layer of alluvium over basalt. We used the Tillotson equation of state, choosing parameters (*21*) for a widely used basalt analog (bedrock) and for alluvium (regolith). The fragmentation parameters of the basalt were derived from (*16*), whereas the alluvium was assumed to be fully fractured (damage = 1). Fragment sizes were calculated, along with shock histories and spall velocities. We performed mesh refinement studies to determine the point at which our results became independent of cell size (Fig. 2). Resolving the shock wave is important, because numerical models typically require artificial viscosity to guarantee that the shock front, which is a few meters wide in geologic materials (*21*), is spread over three cells (*22*). In our simulations, spall velocity is a function of cell size for cells larger than 5 m, indicating that artificial viscosity is important for this choice of cell size. Spall velocity at a given range is constant in our simulations when the cell size is less than 5 m, indicating that a stable solution has been achieved. We interpret this to mean that the high spall velocities are due to the nonlinearities in the Tillotson equation of state (EOS), the effect of which is otherwise masked by artificial viscosity when the cell size is too large. The velocity distribution of the ejected fragments is consistent with earlier work (*23*). The calculation is conducted in two steps. First, an Eulerian calculation is performed to avoid highly distorted cells near the impact. Tracer particles are used to define a velocity boundary condition for the second step, a Lagrangian calculation wherein the material boundaries are at all times well defined, a requisite condition for analyzing spall in the interference zone.

Impact modeling results. The smallest impact capable of producing candidate martian meteorite material was a 150-m-diameter projectile striking a homogeneous basaltic target at 10 km/s (Table 2). The resulting final crater diameter, based on π scaling (*24*) and assuming a factor of 1.25 growth due to crater collapse, is 3.1 km. This is a factor of 4 smaller than diameters produced by previous analytic calculations (*18*). The (pre-atmospheric) simulated fragment sizes are large enough and numerous enough to account for the lherzolitic Shergottites. To produce simulated fragment sizes large enough to account for the remaining Shergottites, the impactor must be larger, about 200 m. The recurrence interval for 3-km craters on Mars is about 200,000 years. If Shergottite material with a crystallization age of less than 400 Ma covers 10% of the martian surface (*25*), than Shergottite-launching events should occur every 2 million years. This is within a factor of 2 of the launch rate apparent in Table 1, within the uncertainties of the current lunar impact flux and the scaling of that flux to Mars (*6*).

When a regolith is introduced, the velocity of the ejected material decreases (Figs. 3 and 4). Hence, a larger impact is required to produce meteorites from such terrain. Currently, the largest impact that we can simulate at our highest resolution of 2.5 m per cell is for a 400-m-diameter projectile. The resulting crater in this simulation is 6.7 km in diameter. It is almost large enough to produce a sufficient number of fragments of the correct size to account for the Nakhlites or Chassigny. Thus, we estimate a lower limit of 7 km for the diameter of the source crater of these meteorites.

Our calculations indicate that the spall from a regolith with a thickness of more than half the impactor diameter is similar in speed and volume to that from a half-space of the same material. On this basis, we assign an estimate of 20 km for the size of the candidate source crater required to eject material from the ancient terrains of Mars. The correlation between the diameter of the source crater and the age of the target material, coupled with the size-frequency distribution of martian craters, are critical factors in explaining the anomalous abundance of young martian meteorites.

Analysis. The small size of the required craters in our simulation is consistent with taking the CRE data as launch ages (*26*). The

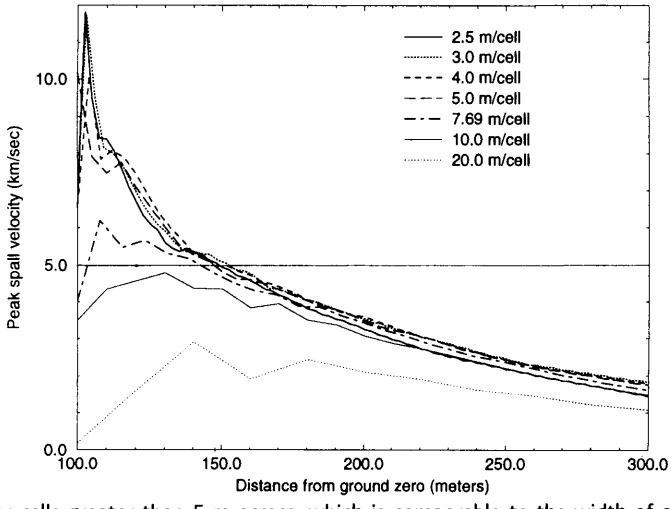

Fig. 2. The figure depicts peak spall velocity as a function of distance from ground zero for seven simulations run under identical conditions, except for the choice of cell size. In these simulations, 100 m is at the edge of the impactor. The figure represents material from inside the final crater, which has a radius of 2 km. Spall velocity decreases rapidly with distance from the impact site. The spall velocity is strongly dependent on the cell size used in the computational grid for cells greater than 5 m across, which is comparable to the width of a shock wave in geologic materials (*22*). However, for cells between 2.5 and 5 m, the spall velocity is nearly constant for any given distance from ground zero, indicating that the simulation has reached a stable solution. The high resolution in the simulation is what allows a consistent prediction of the fast ejecta velocity near the impact site. The 5 km/s escape velocity of Mars is indicated by the horizontal line.

Table 2. Analysis of a 150-m-diameter and a 200-m-diameter, 10 km/s, impact into homogeneous basaltic terrain with a cell resolution of 3.0 and 2.5 m, respectively. In the 150-m impactor event, the estimated crater size is 3.1 km. The majority of the fragments, which have a calculated mean size of 1 cm, are from a single cell. These fragments are too small to be viable martian meteorite progenitors. The largest fragments are comparatively rare. It is unlikely that the Zagami-sized fragments from this impact are numerous enough to expect to find them on Earth, although an event of this scale could account for the lherzolites. In the 200-m impactor event, the estimated crater size is 4 km. The minimum mean fragment size for any cell was 5 cm. This is the main reason why the number of fragments ejected is a factor of ~6 smaller than the smaller impact in this table. Events of this size are large enough to account for the basaltic Shergottites.

150-m-diameter impactor			200-m-diameter impactor		
Size (cm)	Number	Peak pressure (GPa)	Size (cm)	Number	Peak pressure (GPa)
1	2×10^9	40	5–10	1×10^7	40–50
3	6×10^7	40	12–15	1×10^7	20–65
7	4×10^6	45	17–21	2×10^6	20–60
10	8×10^6	65	27–28	2×10^5	30–50
15	5×10^5	35	37	1×10^5	70
26	4×10^5	<30			

recurrence interval for 3-km craters on Mars (200,000 years) provides sufficient opportunity for meteorite ejection events on Shergottite-aged terrain. In addition, the different ages of the meteorites originating from terrains with different regolith thickness is consistent with the CRE data without an ad hoc appeal to small number statistics. A quantitative analysis can be drawn from the available data as shown in Eq. 1

$$N = t_{CRE} \times f_p(D) \times R \times \text{area} \times f_{sfc} \quad (1)$$

where N is the number of source craters on a terrain of a given age, t_{CRE} is the ejection age of the meteorites in question (~4 Ma for Shergottites), and $f_p(D)$ is the lunar crater production function for craters with diameter D or larger. This is 2×10^{-14} craters/km^2/year for 4-km-diameter craters and is scaled to other crater sizes by the slope of the cumulative crater curve for Mars. R is the Mars/Moon impactor flux ratio, "area" is the surface area of Mars (1.45×10^8 km^2), and f_{sfc} is the fraction of Mars covered by terrain of the age of interest. Hence, the number of source craters can be estimated by knowing the minimum size of a source crater; the cratering flux on Mars; the portion of the martian surface covered by terrain of a given age; and the time scale of interest, here assumed to be the launch (CRE) age. The martian cratering flux is assumed to be the same as the lunar flux times a factor R, estimated to be 0.9, with an 3σ uncertainty of about a factor of 2 (*6*). Using these values in Eq. 1, we obtain two to four source craters for the Shergottites, one or two for the Nakhlites and Chassigny, and about one for sample ALH84001. This is consistent with the geochemistry of the martian meteorites.

Running the calculation in reverse, assume exactly four impacts for the Shergottites, two for the Nakhlites and Chassigny, and one for ALH84001. One then computes that 10 to 40% of the martian surface is Shergottite-aged, 10 to 40% is Nakhlite/Chassignite-aged, and 35 to 100% is ALH84001-aged. The factor R accounts for most of the uncertainty (*6*). Obviously, these are constrained to sum to 100% or less; however, these figures are consistent with the estimates of martian terrain ages (*25*). Thus, the hypothesis that the martian meteorites come from a large number of small craters is consistent with all the available chemical and physical constraints. Lunar meteorites require separate consideration (*27*).

It is evident that the recurrence interval from Shergottite-producing impacts is less than the terrestrial delivery time. In contrast, the recurrence interval for ALH84001-liberating impacts maybe longer than the delivery time scale. Hence, one expects to see a steady rain of Shergottite debris, whereas ancient material might derive from single rare impacts. This would imply that crystallization age should be correlated with ejection age, a trait that is observed (Table 1). A closely related point is that small impacts eject relatively highly shocked material as compared to larger impacts, because of the fact that the interference zone (*18*) is larger for larger impacts, meaning that older debris is likely to be launched under gentler shock conditions. This trait is also evident in the meteorites. Another prediction is that additional Shergottites should show older as well as younger CRE ages. Because the model explains the apparent bias in the age of martian samples as an artifact of the launch crater requirements, the crystallization age distribution of the martian meteorites should remain unchanged as more samples are discovered. As the discovery rate is on the order of one every 2 years, in a decade's time we should gather enough new samples to see whether the trend established with the first 13 martian meteorites continues.

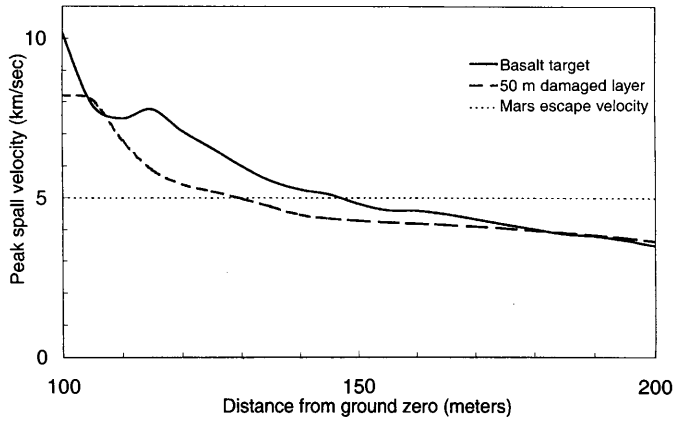

Fig. 3. Spall velocity is suppressed in damaged material. Shown are the peak spall velocities for identical impacts into pristine basaltic material and into pristine basaltic material covered with 50 m of the same material that is fully damaged at the beginning of the simulation. The cells nearest the impactor are highly distorted, hence the spall velocities for the first few vertices are unreliable. Material from this region is excluded from the analysis.

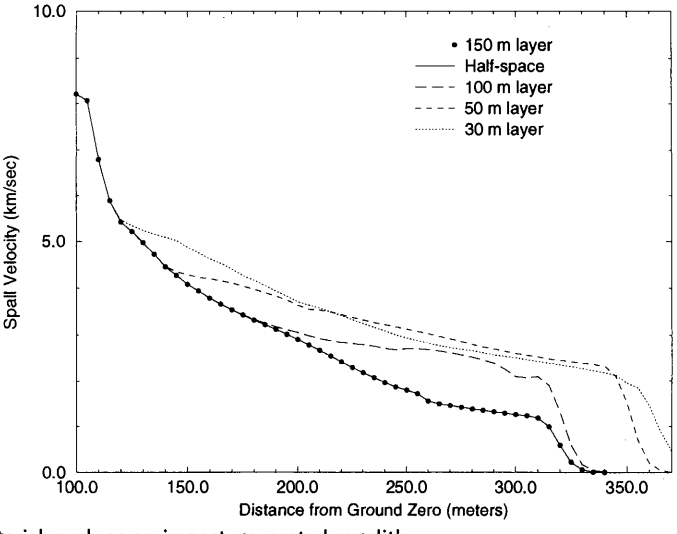

Fig. 4. The thickness of the damaged layer affects the suppression of spall velocity. Here, damage means that the material effectively has a zero shear modulus in tension. The thicker the layer of damaged material (a low-velocity zone), the greater the suppression of the spall velocity. This trend continues until the thickness of the damaged layer is comparable to the impactor radius. This means that a larger impact is required to eject material from terrains overlain by damaged material, such as an impact-generated regolith.

References and Notes

1. A. M. Vickery, H. J. Melosh, *Science* **237**, 738 (1987).
2. L. E. Nyquist, L. E. Borg, C. Y. Shih, *J. Geophys. Res.* **103**, 31445 (1998).
3. C. A. Wood, L. D. Ashwal, *Proc. 12th Lunar Planet. Sci. Conf.* **12B**, 1359 (1981).
4. D. O. Terribilini, M. Eugster, M. Burger, A. Jakob, U. Krahenbuhl, *Meteorit. Planet. Sci.* **33**, 677 (1998).
5. W. K. Hartmann, *Meteorit. Planet. Sci.* **34**, 167 (1999).
6. B. A. Ivanov, in *Chronology and Evolution of Mars*, R. Kallenbach, J. Geiss, W. K. Hartmann, Eds. (Kluwer, Netherlands, 2001), pp. 87–104.
7. A. H. Trieman, *Meteorit. Planet. Sci.* **33**, 753 (1998).
8. ———, *J. Geophys. Res.* **100**, 5329 (1995).
9. P. H. Warren, *Icarus* **111**, 338 (1994).
10. Consider a pristine surface struck by impactors characterized by a cumulative size-frequency distribution known as the production function $f_p(D)$. Because the crater diameter is 20 to 30 times the impactor diameter, the size-frequency distribution of craters on the surface will initially follow that of $f_p(D)$. As craters accumulate, there is a point at which each new crater of a diameter D_{eq} or smaller will on average destroy one old crater, a condition known as saturation or equilibrium. Because of the observed slope of the production function, saturation occurs first at small D_{eq}, then at progressively larger diameters. A surface is said to be saturated to D_{eq} when every point on that surface has a ~100% chance of having experienced an impact event of size D_{eq} or smaller. The impact-generated regolith thickness can be estimated by using scaling relations between D_{eq}, the depth of excavation (about $D_{eq}/4$), and the thickness of the ejecta blanket. Because D_{eq} increases with time, the regolith thickness increases with time. This theory has been validated against seismic studies of regolith thickness on the Moon. For a complete treatment, see (*22*).
11. B. J. Gladman, J. A. Burns, M. Duncan, P. Lee, H. F. Levison, *Science* **271**, 1387 (1996).
12. B. J. Gladman, *Icarus* **130**, 228 (1997).
13. H. Y. McSween, *Meteoritics* **29**, 757 (1994).
14. H. J. Melosh, *Adv. Space Res.* **11**, 87 (1991).

15. A. A. Amsden, H. M. Ruppel, C. W. Hirt, "SALE: A Simplified ALE Computer Program for Fluid Flow at All Speeds" (Report LA-8095, Los Alamos National Laboratory, Los Alamos, NM, 1980).
16. H. J. Melosh, E. A. Ryan, E. Asphaug, *J. Geophys. Res.* **97**, 14735 (1992).
17. J. N. Head, *Eos* **76**, F336 (1995).
18. H. J. Melosh, *Icarus* **59**, 234 (1984).
19. The most common impact angle is 45°, which constitutes an inherently 3D problem that is computationally very expensive. In oblique impacts, the shock wave is stronger down-range and weaker up-range. However, it is still hemispherical and will still weaken as $1/r^2$. Moreover, the propagation of the shock wave will still be affected by the physical nature of the medium (damaged versus undamaged). The azimuthal dependence of shock wave strength might modulate the number of ejected fragments from a crater of a given size, but it should not change our finding that the presence of an impact-generated regolith suppresses spall velocity and hence biases the ejecta launched from Mars in favor of young material.
20. W. F. Bottke Jr., M. C. Nolan, R. Greenberg, R. A. Kolvoord, in *Hazards Due to Comets and Asteroids*, T. Gehrels, Ed. (Univ. of Arizona Press, Tucson, AZ, 1994), pp. 337–357.
21. H. J. Melosh, *Impact Cratering: A Geologic Process* (Oxford Univ. Press, New York, 1989).
22. J. von Neuman, J. D. Richtmyer, *J. Appl. Phys.* **21**, 232 (1950).
23. J. N. Head, H. J. Melosh, *31st Lunar Planet. Sci. Conf.*, abstract 1937 (2000).
24. R. M. Schmidt, K. R. Housen, *Int. J. Impact Eng.* **5**, 543 (1987).
25. K. L. Tanaka, D. H. Scott, R. Greeley, in *Mars*, H. H. Kieffer, B. M. Jakosky, C. W. Snyder, M. S. Matthews, Eds. (Univ. of Arizona Press, Tucson, AZ, 1992), pp. 345–382.
26. In contrast, assume that only 10^6 fragments must be launched from Mars to expect to have one in our meteorite collection and that these fragments derive from a parent fragment undergoing an in-space breakup event. One million 20-cm-diameter stones have a total volume of ~4200 m^3. This is equivalent to a single parent fragment 20 m across. Such a large fragment would have to come from a much larger and therefore much rarer impact than the ones modeled here. Consider further that to create a large number of different CRE ages, this fragment must undergo multiple breakup events, or a group of such mother fragments must each undergo breakup events at different times. Moreover, consider a 10-m-radius ejecta fragment as the parent of eight Shergottites. If the cosmic ray shielding depth is 2 m, then about half the volume of the fragment is shielded and will not present a 2-π exposure history. A random draw of eight stones from the entire fragment would then have a $(1/2)^8$ or 1/256 chance of all stones presenting a single-stage CRE history. Because multiple ages are required, and at each step the ratio of two-stage to single-stage CRE history material increases, the odds for recovering only 4-π exposed stones drops even more. Finally, an impact that launches a 20-m-diameter fragment will likely launch an enormous number of decimeter-scale fragments, which would be more likely to reach Earth than would pieces of the 20-m fragment (*28*).
27. The data in Fig. 3 show that a low-velocity regolith layer may be irrelevant with regard to launching lunar meteorites because of the much lower lunar escape velocity of ~2.3 km/s. At this value, the spall velocity is the same in our models regardless of the presence of a regolith layer. The launch efficiency is then the same whether the surface is pristine or a deep regolith. Hence, the mechanism by which the launch of martian meteorites is biased in favor of young material cannot operate on the Moon. One implication of this is that lunar meteorite petrology should be representative of the observed surface units. This appears to be the case (*9*). The delivery time scale is much less than for martian meteorites, and the maximum terrestrial age is evidently ~0.1 Ma. This implies that meteorites found on Earth are predominately from the most recent lunar impacts, because samples from older impacts would have been destroyed long ago by the terrestrial environment. As a test of our model, we simulated lunar meteorite launch, modeling the lunar surface as basaltic covered by a regolith of the same material, but damaged. We found that the expected number of source craters is consistent with that estimated from the lunar meteorites in hand, but only for impacts that are recent compared to the Moon-to-Earth delivery time scale. Samples from older impacts appear to be greatly underrepresented in the meteorite collection with regard to our model results. The few lunar meteorites with launch ages greater than a few hundred thousand years (up to ~10 Ma) are found only if they have been sequestered in the relatively benign space environment for most of their post-launch history (*29*).
28. G. W. Wetherill, *Meteoritics* **19**, 1 (1984).
29. J. N. Head, *32nd Lunar Planet. Sci. Conf.*, abstract 1768 (2001).
30. R. Score, M. M. Lindstrom, *Antarct. Meteorite Newsl.* **13** (1990).
31. C. Satterwhite, B. Mason, *Antarct. Meteorite Newsl.* **14** (1991).
32. R. Score, B. Mason, *Antarct. Meteorite Newsl.* **18** (1995).
33. H. Kojima, M. Miyamoto, P. H. Warren, *Antarct. Meteorite Res.* **10**, 3 (1997).
34. J. N. Grossman, *Meteorit. Planet. Sci.* **34**, A169 (1995).
35. K. Nagao, T. Nakamura, Y. N. Miura, N. Takaoka, *Antarct. Meteorite Res.* **10**, 125 (1997).
36. E. O. Jagoutz, O. Bodganovski, N. Krestina, R. Jotter, *30th Lunar Planet Sci. Conf.*, abstract 1808 (1999).
37. F. Langenhorst, A. Greshake, *Meteorit. Planet. Sci.* **34**, 43 (1999).
38. M. Eugster, A. Weigel, E. Polnau, *Geochem. Cosmochim. Acta* **61**, 2749 (1997).
39. L. Folco, I. A. Franchi, P. Scherer, L. Schultz, C. T. Fillinger, *Meteorit. Planet. Sci.* **34**, A36 (1999).
40. K. Nishiizumi *et al.*, *30th Lunar Planet Sci. Conf.*, abstract 1966 (1999).
41. The authors acknowledge helpful reviews, which improved the quality of this paper.

19 August 2002; accepted 24 October 2002
Published online 7 November 2002;
10.1126/science.1077483
Include this information when citing this paper.

REPORTS

Formation of Giant Planets by Fragmentation of Protoplanetary Disks

Lucio Mayer,[1*†] Thomas Quinn,[1*] James Wadsley,[2] Joachim Stadel[3†]

The evolution of gravitationally unstable protoplanetary gaseous disks has been studied with the use of three-dimensional smoothed particle hydrodynamics simulations with unprecedented resolution. We have considered disks with initial masses and temperature profiles consistent with those inferred for the protosolar nebula and for other protoplanetary disks. We show that long-lasting, self-gravitating protoplanets arise after a few disk orbital periods if cooling is efficient enough to maintain the temperature close to 50 K. The resulting bodies have masses and orbital eccentricities similar to those of detected extrasolar planets.

About 100 extrasolar planets have been detected by the wobble they induce on their star (*1*, *2*). Their masses range from about one Jupiter mass (M_J) to more than 10 M_J and have orbits ranging from nearly circular to very eccentric. In the standard core-accretion model, giant planets might require longer than 10^6 years to form (*3*, *4*), which could exceed observed disk lifetimes (*5*–*7*). In particular, more than 80% of the stars in the Galaxy probably formed in dense clusters like those in the Orion nebula (*8*) where the ultraviolet radiation of bright stars can ablate the gaseous disk in far less than a million years (*5*, *6*). Hence giant planet formation must occur quickly, or such planets would be rare. Even in the case where a large solid core is assembled rapidly enough, torques acting between the disk and the protoplanets are believed to induce its complete inward migration in a few thousand years (*9*, *10*). Planets could therefore sink toward the star before being able to accrete the large gaseous masses observed (*11*, *12*). Alternatively, giant planets could coagulate directly in the gas component as a result of gravitational instabilities in a cold disk with a mass comparable to that adopted in the core-accretion model (*13*, *14*). Simulations done with codes that solve the hydrodynamical equations on a fixed grid show that slightly perturbed disks form strong spiral arms and overdensities at $R > 10$ astronomical units (AU) (*15*, *16*) where the temperature can be lower than 60 K (*17*, *18*). The trigger of the instability might come from material of the protostellar cloud infalling onto the disk (*13*). If these condensations are long-lasting and can contract to planetary densities, gravitational instability would be the prevailing formation mechanism for giant planets because it takes less than a thousand years (*13*, *15*). Solid cores with masses as low as currently esti-